chemistry

MDPI

Article

Tetrakis(oxadiazolyl)benzenes and -Pyrazines: Novel Fluorescent Cruciform Liquid Crystals †

Vincent Graschtat [1], Nico Achenbach [1], Matthias Lehmann [2] and Heiner Detert [1,*]

[1] Department of Chemistry, Johannes Gutenberg University Mainz, 55099 Mainz, Germany
[2] Institute of Organic Chemistry, University of Würzburg, 97074 Würzburg, Germany; matthias.lehmann@uni-wuerzburg.de
* Correspondence: detert@uni-mainz.de
† Dedicated to Prof. Herbert Meier, Mainz, on the occasion of his 87th birthday.

Abstract

This study investigates the fluorescent and mesomorphic properties of tetrakis(oxadiazolyl)benzenes (TOBEs) and -pyrazines (TOPYs), novel cruciform liquid crystals. The impact of a set of four side chains on optical and mesomorphic properties is reported. TOBE absorbs in the UV range (~360 nm), while substituting the central benzene ring by pyrazine (TOPY) shifts the absorption maximum to 396 nm but lowers the fluorescence quantum yield (TOBE: 72%; TOPY: 21%; in toluene). Fluorescence in the green-to-orange range is influenced by solvent polarity. Mesophase analysis shows quite narrow phases (~20 K) for TOBE. As the pyrazine core lowers the melting point and elevates the clearing temperature, huge mesophase ranges (~80–90 K) are detected for TOPY. Side chain variations further influence material properties: TOBE with linear alkyl chains exhibits multiple crystal–crystal transitions, while branching enhances mesophase stability and alters fluorescence characteristics. The Huisgen reaction provides a cost-effective synthetic route for these fluorescent mesogens, offering high yields and efficiency.

Keywords: liquid crystals; cruciform; sensing; heterocycles; fluorescence

1. Introduction

In recent years, discotic liquid crystals (DLCs) composed of a central ring and conjugated arms were prepared and investigated as electronic materials, e.g., in organic light-emitting diodes (OLEDs), organic field-effect transistors (OFETs), and organic photovoltaic cells (OPVs) [1–7]. Among them, cruciform or "X-shaped" molecules have attracted substantial attention for their promising application in optoelectronic devices. Due to their two-dimensional π-conjugated frameworks, these cruciform mesogens, unlike traditional calamitic or discotic liquid crystals, offer exciting potential for advancing the efficiency and performance of optoelectronic devices [1–7].

Earlier studies have shown that the charge transport properties of organic molecules are strongly influenced by their orientation, with molecules showing a highly ordered superstructure exhibiting higher charge carrier mobility [8,9]. X-shaped molecules are generally expected to exhibit superior ordering compared to rod-shaped structures [10–13]. In these molecules, the conduction of excess charge occurs in two dimensions, enhancing the rate of charge transport between molecules. Charge transport analysis of various X-shaped molecules confirms high charge carrier mobility, further supporting their potential for optoelectronic applications [12].

Academic Editor: Feng Long Gu

Received: 15 July 2026
Revised: 18 August 2026
Accepted: 26 August 2026
Published: 29 August 2026

Research performed in the early 21st century, e.g., by Kim [14], Blanchard-Desce [15,16], Meier [17], Imrie [18], Zhang [19], Goodby [20] and us [5,21], led to the development of multi-arm liquid crystals (LCs) with enhanced mesophase properties. The multi-arm design results in wider mesophase ranges due to lower melting points and higher clearing points compared to traditional small-molecule LCs. For example, tetraester-based star mesogens (Figure 1), based on a tetrahydroxybenzene core and semi-flexible oligobenzoate arms (**1**), demonstrate broad mesophases [5]. Structural modifications are the key to tuning the mesomorphic behavior and thermal stability of cruciform mesogens. For example, the partial fluorination of 1,2,4,5-tetra((alkoxyphenyl)ethynyl)benzene (**2**) by Wu [4] stabilizes the nematic phase by both lowering transition temperatures and broadening the mesophase range.

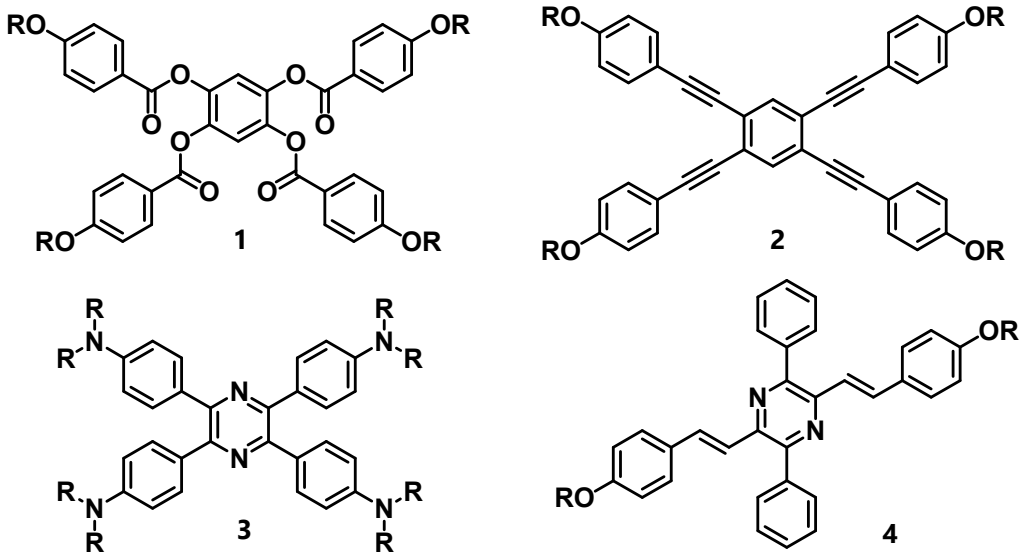

Figure 1. The literature examples of cruciform mesogens with a central benzene ring (**1**,**2**) [5,22] or pyrazine (**3**,**4**) [23,24].

Applying advanced computational methods like (time-dependent) density functional theory ((TD)-DFT), Senthilkumar et al. [12] provided valuable insights into structural modifications influencing the optoelectronic properties of cruciform mesogens. By strategically incorporating electron-donating (EDGs) and electron-withdrawing groups (EWGs), the electron density distribution can be finely tuned, which directly impacts fluorescence and charge transport properties. Addition of electron-withdrawing substituents stabilizes the excited state and promotes two-photon absorption, while electron-donating groups increase HOMO electron density, optimizing fluorescence [25]. Bunz [23,24] reported amino-cruciforms with a high potential for use for sensing purposes. Similarly, optical properties of donor-substituted X-shaped distyrylpyrazines [26] (**5**) and similar quadrupolar D-A cruciforms from Zang [27] are highly sensitive to their environment. This responsiveness is attributed to the electronic interactions between the core and the electron-pair-donating groups, which modulate the conjugated π-system. Gong et al. [28] explored the design and synthesis of cruciform donor–acceptor (D-A) conjugated chromophores derived from tetraphenylpyrazine (Figure 1, **3**). The tetraphenylpyrazine core is known for its aggregation-induced emission (AIE) properties and structural flexibility [3].

While a huge number of DLCs with C_2, C_3, C_4 and even C_6 symmetry have been synthesized [1,29,30] and studied in detail, there are only a quite limited number of St Andrews cross-shaped DLCs with D_2h symmetry [31–36]. These are made from different core and arm components, but they all share a relatively high electron density due to

donor substitution. On the other hand, Bock studied DLCs with pyrene- and coronene-carrying ester groups as EWGs [37,38], and we reported tetrakis(phenyloxadiazolylphenyl)-pyrazines (TOPPs) [21], cruciform mesogens with highly electron-deficient heterocycles as building blocks.

This study focuses on the synthesis and characterization of novel fluorescent D_2h symmetrical cruciforms, tetrakis(phenyl-1,3,4-oxadiazolyl)benzenes (TOBEs) and -pyrazines (TOPYs), and their mesomorphic and optical properties. These discotic liquid crystals are designed to exhibit enhanced fluorescence and mesophase stability, key factors for determining promising candidates for next-generation optoelectronic devices [28]. Through the integration of four central oxadiazoles, both TOBEs and TOPYs stand out as rare examples of electron-deficient cruciform LCs.

2. Synthesis

The syntheses of tetrakis(oxadiazolyl)benzenes (TOBEs) and -pyrazines (TOPYs) as cruciform liquid crystals rely on a convergent approach using a fourfold Huisgen reaction [39–41] as the core synthetic step. This method yields high-purity products and simplifies the work-up process, as recrystallization is sufficient to isolate the final compounds, eliminating the need for costly and time-intensive column chromatography.

Traditional syntheses of 1,3,4-oxadiazoles typically require a multi-step process involving the formation of diacylhydrazines, followed by dehydration/cyclization using highly aggressive $POCl_3$ [42,43]. In contrast, the Huisgen reaction directly couples acyl chlorides and tetrazoles in the presence of a base to form acyltetrazoles. These intermediates eliminate nitrogen and cyclize to the desired 1,3,4-oxadiazoles in a single synthetic step (Scheme 1). The main advantage of the Huisgen route is the efficient synthesis of sensitive compounds [44], making it an ideal approach for the synthesis of fluorescent mesogens.

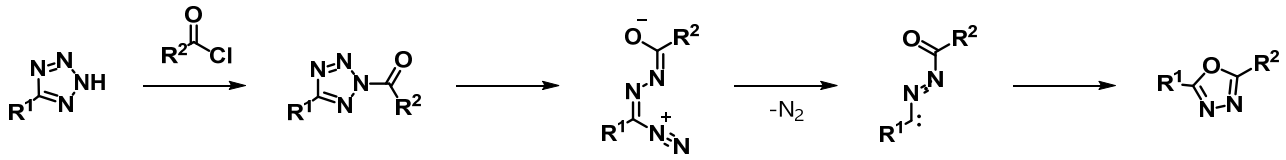

Scheme 1. Mechanism for the conversion of tetrazoles to 1,3,4-oxadiazoles.

The required tetrazoles (**7**) were synthesized by alkylating protocatechuic nitrile (**6**) to produce 3,4-dialkoxybenzonitriles, followed by a 1,3-dipolar cycloaddition with sodium azide (Scheme 2). The combination of sodium azide and aluminum chloride in *N*-methyl-2-pyrrolidone (NMP), as described by Kappe et al. [45], significantly enhanced the tetrazole formation with slightly increased yield. The pyrazine core was synthesized by $KMnO_4$ oxidation of tetramethylpyrazine according to Dürr et al. [46]. This method produces highly pure pyrazine tetracarboxylic acid (**8**), which serves as central building block for the targeted electron-deficient cruciforms.

The final TOBE and TOPY compounds were synthesized by converting either pyromellitic acid **9** or pyrazine tetracarboxylic acid **8** into the corresponding acid chloride using thionyl chloride. The crude acid chloride was directly subjected to the Huisgen reaction with aryltetrazole **7**. Both the acid chlorides **8** and **9** and tetrazole **7** were dissolved in toluene, with diisopropylethylamine (DIPEA) added as the base. The reaction mixture was heated overnight; the desired products were obtained at high yields of up to 82% (Table 1). Unlike pyridine bases [40,47], which led to undesirable side products, DIPEA facilitated a clean reaction, as confirmed by TLC monitoring. This synthetic pathway provides quick and easy access to stable, fluorescent TOBE and TOPY cruciform liquid crystals **10–17**. Synthetic details and analyses are given in the supporting information.

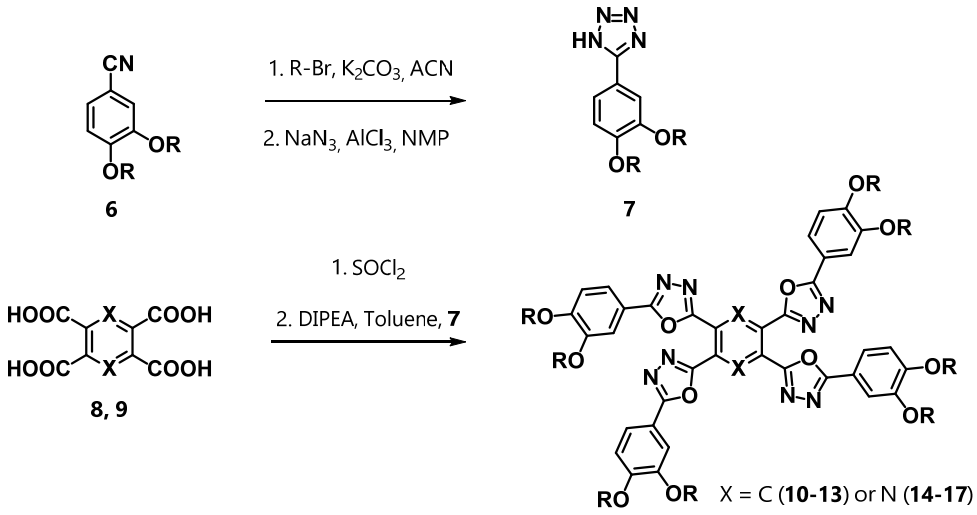

Scheme 2. Reaction procedure for the synthesis of TOBE **10–13** and TOPY **14–17**.

Table 1. Synthesized TOBEs and TOPYs, with their substituent patterns and yields.

Compound	X	R	Yield [%]
10	C	C_8H_{17}	53
11	C	$C_{10}H_{21}$	19
12	C	$C_{12}H_{25}$	16
13	C	3,7-dimethyloctyl	43
14	N	C_8H_{17}	76
15	N	$C_{10}H_{21}$	63
16	N	$C_{12}H_{25}$	82
17	N	3,7-dimethyloctyl	34

3. Thermal Properties: DSC and POM

Polarized optical microscopy (POM) investigations of tetrakis(oxadiazolyl)benzenes (TOBEs) and -pyrazines (TOPYs) revealed birefringent mesophases for all compounds. The fan-shaped or pseudo-focal conical textures (Figure 2) are typical of discotic liquid crystals [30,48]. Furthermore, these textures are in agreement with the hexagonal columnar nature of the mesophases, as analyzed by WAXS (*vide infra*). Shearing experiments confirmed that TOBE and TOPY exhibit high viscosity in their respective mesophases, indicating strong intermolecular interactions within the columnar stacking.

Differential scanning calorimetry (DSC) provided further insight into the thermal properties of the cruciform liquid crystals, revealing interesting mesomorphic properties for both TOBE and TOPY compounds (Figure 2, Table 2). Specifically, TOBEs exhibited mesophase widths of approximately ΔT = 14 to 50 K, whereas the pyrazine derivatives demonstrated significantly broader ranges, even extending up to ΔT = 85 K. This pronounced difference in thermal behavior suggests that TOPYs possess higher column stability. The broader mesophase range observed in TOPYs is likely attributed to the electronic influence of the pyrazine core, which incorporates additional nitrogen atoms with lone pair electrons, altering the electronic environment. Electron-rich sites in the mean plane induce intracolumnar repulsive forces. Consequently, this repulsion disrupts the π-π stacking interactions, which prevents close packing and results in a more dynamic system. As a result, TOPYs exhibit lower melting points. This and the slightly higher clearing points compared to their benzene counterparts result in wider mesophases. These findings highlight the suitability of nitrogen-rich heterocycles as liquid crystal cores and are also in alignment with our previous studies on tris(aryl-1,3,4-oxadiazolyl)triazines (TOTs) [44], where the triazine-based

mesogens also showed enhanced mesophase stability compared to analogous carbon-based systems (TOBs).

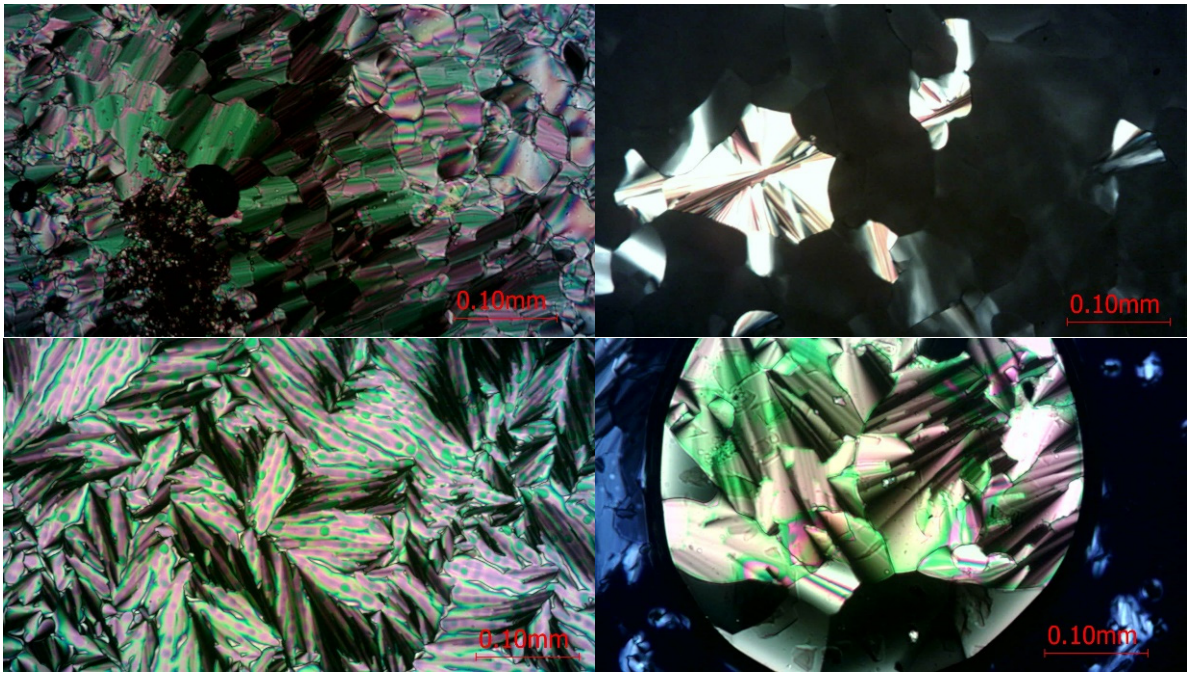

Figure 2. POM images of TOBE **10** (**top left**) and **13** (**top right**), and TOPY **14** (**bottom left**) and **15** (**bottom right**).

Table 2. Phase transition temperatures and enthalpies of TOBEs and TOPYs. Temperature values are given as onset signals of the second heating curve.

Compound	T_m * [°C]	Δ*H* [kJ/mol]	T_C * [°C]	Δ*H* [kJ/mol]
10	146.9	17.9	160.3	7.1
11	136.2	25.9	158.3	8.0
12	130.9	72.0	183.6	0.9
13	98	28.9	123.2	7.6
14	108.1	43.4	189.9	10.3
15	99.8	33.4	188.0	9.2
16	91.5	35.4	176.3	9.6
17	97.6	16.0	/	/

* Onset signals of second heating curve.

TOBE derivatives with linear alkyl chains showed multiple crystal–crystal transitions, observed as a series of broad transitions in the DSC scans (Figure 3, left). This behavior is analogous to previous findings on C_3-symmetric tris(aryl-1,3,4-oxadiazolyl)benzenes (TOBs) [34]. Notably, some TOBE compounds exhibit exothermic transitions during the second heating cycle, attributed to thermally induced crystallization. Upon cooling, the material remains in a metastable phase, which persists when frozen. Upon reheating, the introduction of energy induces cold crystallization, as evidenced by the large exothermic peak just before the melting point in the second heating cycle (Figure 3, left).

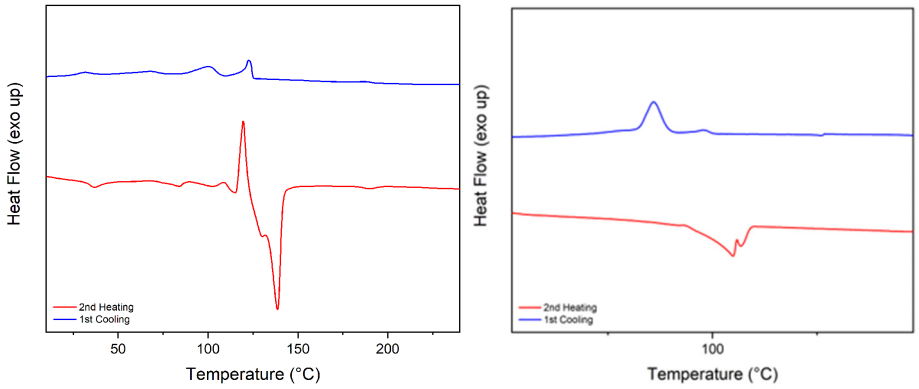

Figure 3. DSC: TOBE **12**, with crystal–crystal transitions noticeable by broad signals and a high-temperature columnar liquid crystal (**left**); TOPY **17,** which only forms a soft crystalline phase (**right**).

In contrast, TOBE **13** with branched alkyl chains did not display these transitions, potentially due to steric hindrance within the stacking pattern introduced by the branched chains. Additionally, this branching created diastereomeric mixtures resulting from the introduction of chiral centers that may have inhibited proper stacking and resulted in limited mesomorphism [49].

The mesophase ranges of the pyrazine derivatives are remarkably consistent (Table 2); DSC scans give only two transitions (ESI). Compound TOPY **15**, functionalized with decyl chains, displayed the broadest mesophase range. This likely resulted from the optimal balance between core rigidity and the flexibility of the decyl side chains, allowing for enhanced molecular alignment and stability of the columns in the liquid crystalline state.

The branched derivative **17** exhibits unique textural properties, distinctly different from the other textures. POM investigation reveals a pseudo-focal conical fan texture, interspersed with a striped texture. Upon heating, this texture softens and shows slight shearability, more indicative of a soft crystal than a classical liquid crystal phase. This observation is further supported by DSC (Figure 3, right), which displays only a single broad thermal transition. This behavior suggests that the branched structure may disrupt the molecular packing necessary for typical liquid crystalline phases, leading instead to a phase with intermediate characteristics.

A comparative analysis of the mesomorphic properties of tetrakis(oxadiazolyl)benzenes and -pyrazines reveals distinct trends consistent with observations from similar compounds reported previously [21,44]. Carbon-based TOBEs display narrow mesophase ranges, whereas their pyrazine counterparts show significantly broader mesophases, e.g., TOBE **11**: 22K versus TOPY **15**: 88K. Additionally, the carbon-centered systems show multiple crystal–crystal transitions.

Compared to C_3-symmetrical star-shaped compounds with three aryloxadiazolyl arms, TOBEs and TOPYs exhibit higher melting points and smaller mesophase ranges [34]. Like for TOBEs/TOPYs, stars with a 1,3,5-triazine center melt at lower temperatures than their benzene counterparts. Furthermore, the melting points of λ-shaped 1,2,4-(triaryloxadiazolyl)benzenes are slightly below those of analogous cruciform molecules, but their mesophases are very narrow [50].

The LC structures of the representative compounds TOBE **11** and TOPY **15** were investigated on macroscopically aligned fibers using two-dimensional wide-angle X-ray scattering (WAXS). The specimens were prepared via extrusion at 140 °C for **11** and 110 °C for **15**. WAXS patterns were recorded upon heating in narrow temperature increments to identify the LC phase (Figure 4). At 145 °C, **11** exhibited an aligned X-ray pattern characteristic of a columnar LC phase, indicated by a strong 10 reflection and a broad halo. The presence of characteristic optical textures and a transition enthalpy of 7.9 kJ/mol

further supports the assignment to a columnar LC phase within a narrow temperature range. Although the 11 and 20 reflections remained undetected, the combined observed features (POM, DSC, WAXS) were consistent with a hexagonal columnar structure, the lowest ordered columnar LC phase. Assuming hexagonal symmetry, the columnar lattice parameter was calculated to be a_h = 3.24 nm. The meridional halo indicated an average hydrocarbon chain separation of 0.46 nm. There was only a very broad shoulder at the wide-angle side of the halo pointing to rather disordered π-π stacking for compond **11**.

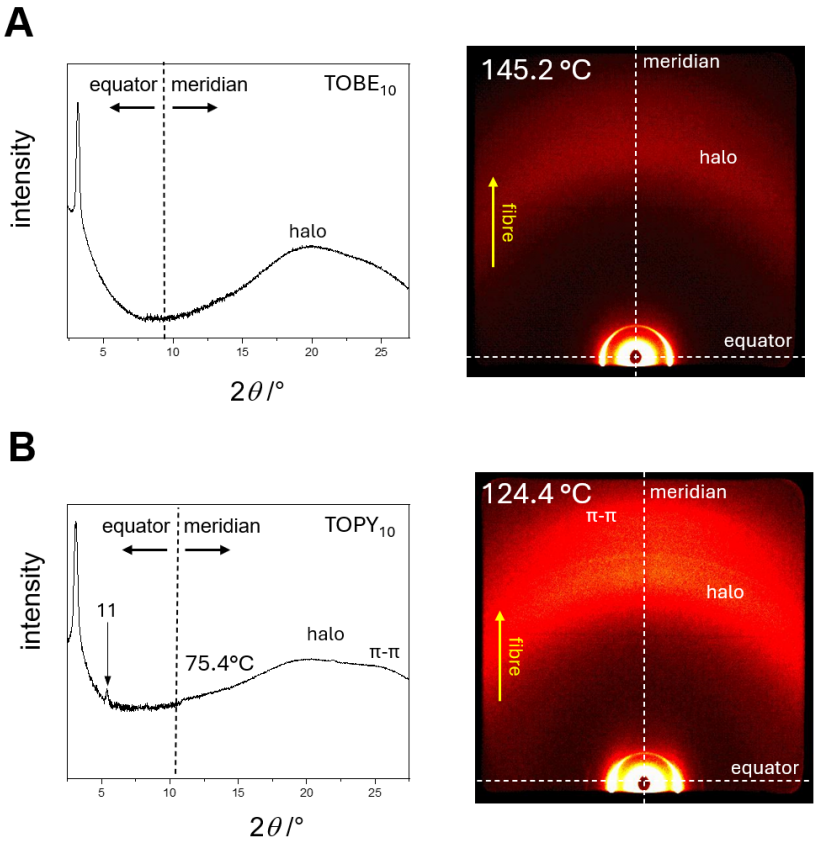

Figure 4. Diffraction pattern and integration along the equator/meridian for TOBE **11** (**A**) and TOPY **15** (**B**).

Structural data for pyrazine-centered **15** was obtained on a macroscopically aligned fiber at 124 °C. Reflections on the equator indexed as 10 and 11 confirmed a hexagonal columnar phase with a_h = 3.28 nm. Two distinct meridional signals corresponded to the average distance between liquid-like aliphatic chains (halo at 0.46 nm) and π-π stacking, which was not well-defined, similar to material **11**. This clearly confirms the liquid-like columnar nature of the studied compounds.

4. Absorption and Emission Properties

TOBEs and TOPYs are yellow-to-orange solids with fluorescence in the green-to-orange range. The optical properties of the decyl derivatives **11** and **15** are investigated as representative compounds. In solution, the absorption maxima of TOBEs peak around λ_{max} = 363 nm; due to the more pronounced donor–acceptor structure in TOPYs, their absorption maxima appear at lower energies, such as λ_{max} = 393 nm. Similarly, the corresponding fluorescence of **11** appears at higher energies than that of the pyrazine counterparts (Table 3). Unlike absorption, fluorescence depends strongly on the nature of the solvents.

Table 3. UV-Vis and fluorescence spectroscopy in solutions of **11** and **15**.

	Solvent	λ_{max}^{abs} /nm	ε /Lmol^{-1} cm^{-1}	λ_{max}^{Fl} /nm	$\Delta\bar{\nu}^{St}$ /cm^{-1}	Φ_F %
11	cyclohexane	365	5.76×10^4	442	4747	42
	toluene	363	5.46×10^4	470	6249	72
	dichloromethane	362	4.86×10^4	508	7939	28
15	cyclohexane	388	5.62×10^4	472	4564	13
	toluene	395	4.98×10^4	512	5766	21
	dichloromethane	391	4.96×10^4	570	8016	1

TOBE **11** and the pyrazine counterpart **15** emit λ_{max} in the range of 440 up to 570 nm (Figure 5). Solvent polarity strongly affects the fluorescence wavelength and quantum yields, with the pyrazine derivative being slightly more sensitive (Figure 5). Comparing solutions in cyclohexane and dichloromethane, positive solvatochromism shifts the emission maximum of **11** about $\Delta\nu = 2939$ cm^{-1} and of **15** about $\Delta\nu = 3642$ cm^{-1} to lower energies; concomitantly, the Stokes shift, the difference between absorption and emission maxima, reaches $\Delta\nu = 8000$ cm^{-1}, and the fluorescence quantum yields decrease. Here again, the pyrazine derivative is much more sensitive.

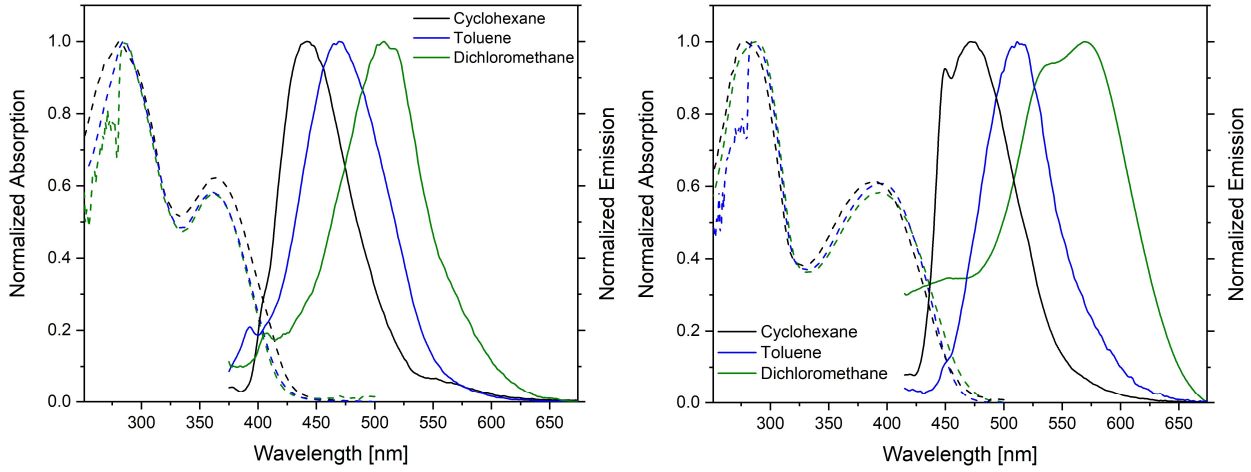

Figure 5. Spectroscopic data of **11** (**left**) and **15** (**right**) in various solvents. Normalized absorption (dashed) and normalized emission (solid).

Regarding fluorescence quantum yields, both **TOBEs** and **TOPYs** demonstrate significant dependence on solvent polarity (Table 3). In non-polar solvents, **TOBEs** achieve fluorescence quantum yields as high as 72%, while **TOPY** derivatives reach quantum yields up to 21%.

The structure of the aliphatic side chains has no influence on the electronic states of the chromophore in dilute solutions. Absorption and fluorescence characteristics of TOBEs **11** and **13** are essentially identical (λ_{max} = 442 nm in cyclohexane). In the solid state, the side chains affect packing and can control intermolecular interactions (Figure 6). Notably, **11** (λ_{max} = 488 nm) exhibits a substantially larger hypsochromic shift in the solid state compared to **13** (λ_{max} = 465 nm, ESI). The fluorescence blueshift is attributed to the changed non-polar environment in the LC phase. The branched side chains in **13** introduce steric hindrance, impairing close molecular packing, reducing intermolecular interactions, and altering the electronic transitions of the fluorophores. Furthermore, the impact of branching

on aggregation—and therefore on the optical properties of the solid materials—is visible upon thermal treatment (Figure 7). Whereas the emission maxima of the pristine spin-coated films of **11** and **13** deviate by Δλ = 23 nm, annealing of **11** results in a hypsochromic shift of Δλ = 14 nm, and the emission of **13** is shifted bathochromically (Δλ = 15 nm); thus, nearly identical emission maxima were recorded. Annealing of the disordered freshly spin-coated film results in the self-assembly of the columnar structure. Interestingly, the branched chain compound **13** seems to need much more time for this process.

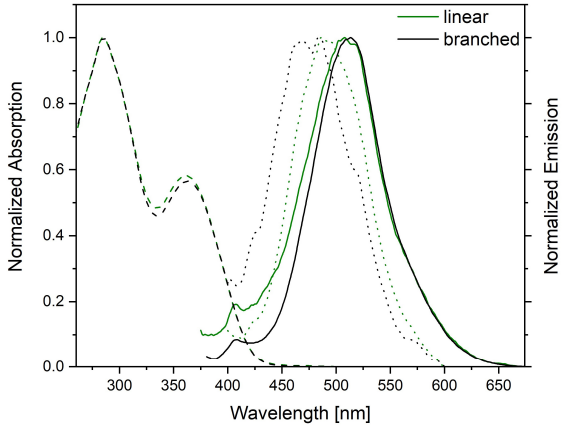

Figure 6. Comparison of spectroscopic properties of **11** and **13**. Normalized absorption in DCM (dashed), normalized emission in DCM (solid), and normalized emission in spin-coated film (dotted).

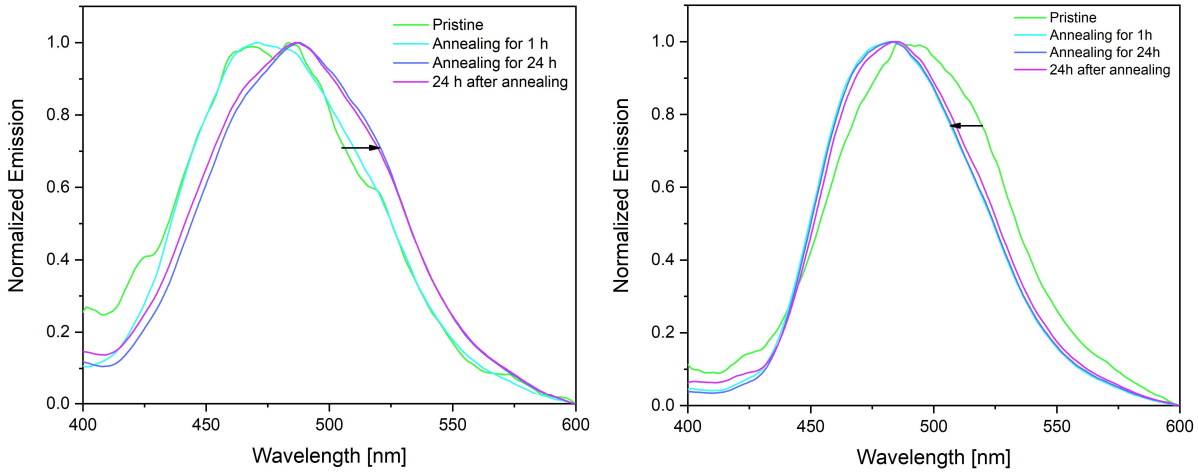

Figure 7. Annealing experiment of spin-coated films of **11** (**left**) and **13** (**right**). Hypsochromic and bathochromic shifts after annealing are indicated by arrows.

Significant differences emerge when comparing the solid-state fluorescence properties of TOBE **11** and TOPY **15**. Compound **15** is not emissive in the solid state, likely attributable to aggregation-caused quenching (ACQ). Conversely, TOPY **17** is emissive in the solid state (λ_{max} = 495 nm); annealing, even for 24 h, displays only a minimal hypsochromic shift. This indicates that the non-mesomorphic nature of **17** prohibits changes in the structure and fluorescence persists by preventing the formation of non-emissive aggregates.

In the following, both the absorption and emission of the cruciform TOBE **11** are compared with those of the linear model compound **18**. The cruciform chromophore of TOBE can be regarded as the linear 1,4-bis(aryl-1,3,4-oxadiazolyl)benzene chromophore **18** (ESI) with two additional aryl-1,3,4-oxadiazolyl arms in the 2,5-positions of the central ring. The absorption maximum of **11** appears at λ_{max} = 363 nm, an only 23 nm higher wavelength compared to the linear model compound **18** (λ_{max} = 340 nm). Contrary to excitation, the

double *ortho*-conjugation in **11** has a much stronger effect on the fluorescence maximum (λ_{max} = 508 nm, CH_2Cl_2), red-shifted about $\Delta\nu$ = 3146 cm^{-1} relative to **18** (λ_{max} = 438 nm, CH_2Cl_2). The solvatochromic shift in the emission of model compound **18,** $\Delta\nu$ = 2939 cm^{-1}, is slightly weaker than that of TOBE ($\Delta\nu$ = 2549 cm^{-1}, C_6H_{12} to CH_2Cl_2). It appears that excitation is mainly controlled by the linear five-ring segment, whereas the excited state involves the entire molecule.

5. Conclusions

This study on the cruciform liquid crystal tetrakis(oxadiazolyl)benzenes (**TOBEs**) and -pyrazines (**TOPYs**) reveals their potential for optoelectronic applications by investigating their fluorescence and mesomorphous properties.

TOBEs and TOPYs are fluorescent chromophores with absorption in the UV (~360 nm for TOBEs) or blue region (~396 nm for TOPYs). These compounds emit in the green-to-orange range with high quantum yields in solution and pronounced positive solvatochromism.

The widths of the mesophases of TOBEs are moderate, exceeding 50 K for TOBE **12**, while TOPYs show much broader ranges (up to 85 K). The pyrazine core contributes to lower melting points and higher clearing points, making mesophases of TOPYs more stable. The side chain also plays a critical role: linear alkyl chains in TOBEs exhibit multiple crystal–crystal transitions, whereas branched chains (**13**) enhance mesophase stability by impairing aggregation, resulting in defined mesophase transitions and bathochromic shifts in fluorescence in the solid state. On the other hand, TOPYs with linear chains do not fluoresce in the solid state but branching of the side chains results in a solid-state fluorophore.

The Huisgen reaction provides an efficient synthetic route, offering high yields and cost-effectiveness for producing high-quality mesogens. In conclusion, the fluorescence properties and mesophase stability of TOBEs and TOPYs make them ideal candidates for use in OLEDs, OFETs, and other optoelectronic technologies.

Supplementary Materials: The following supporting information can be downloaded at: https://www.mdpi.com/article/10.3390/chemistry8090119/s1, Synthetic details and analyses of compounds **6a–6d**, **7a–7d**, [51] **8**, **10–18**; Table S1: POM textures; Table S2: Phase transition temperatures; Table S3: UV-Vis- and Fluorescence Spectroscopy in solution of **11**, **13**, **15**; Figures S1–S18: ^{1}H- and ^{13}C-NMR spectra of **6a–6d**, **7a–7d**, **8**, **10–18**; Figure S19: star-like mesogens reported [21,44]. Figures S20–S27: DSC of **10–17**; Figure S28: Spectroscopic data of **11**; Figure S29: Spectroscopic data of **14**; Figure S30: Annealing experiment of spin-coated film of **11**; Figure S31: Annealing experiment of spin-coated film of **13**; Figure S32: Comparison of spectroscopic properties of **11** and **13**; Figure S33: Annealing experiment for spin coated film of **13**; Figure S34: Absorption (dashed) and fluorescence spectra (solid) of compound **18**; Figure S35: Diffraction pattern and integration along the equator/meridian for **11** (**A**) and **13** (**B**).

Author Contributions: Conceptualization, H.D. and V.G.; methodology, H.D. and V.G.; synthesis, V.G. and N.A.; X-ray, V.G. and M.L., spectroscopy, V.G. and N.A., funding, H.D.; writing, V.G., H.D. and M.L. All authors have read and agreed to the published version of the manuscript.

Funding: The project was co-financed by the Deutsche Forschungsgemeinschaft DE 515-12.

Data Availability Statement: The original contributions presented in the study are included in the article and Supporting Information, further inquiries can be directed to the corresponding author.

Conflicts of Interest: The authors declare no conflicts of interest.

References

1. Detert, H.; Lehmann, M.; Meier, H. Star-shaped conjugated systems. *Materials* **2010**, *3*, 3218–3330. [CrossRef]
2. Devadiga, D.; Ahipa, T.N.; Bhat, V.; Kumar, S. Dimeric cyanopyridine with methylenebis (oxy)-based linker: A tactic to luminescent molecules exhibiting room temperature liquid crystalline property. *Dye. Pigment.* **2023**, *220*, 111695. [CrossRef]
3. Chen, H.H.; Lin, H.A.; Lai, Y.H.; Lin, S.Y.; Chiang, C.H.; Hsu, H.F.; Shih, T.L.; Lee, J.J.; Lai, C.C.; Kuo, T.S. Enantiotropic Nematics from Cross-like 1,2,4,5-Tetrakis(4′-alkyl-4-ethynylbiphenyl)benzenes and Their Biaxiality Studies. *Chem. Eur. J.* **2012**, *18*, 9543–9551.
4. Lin, Y.H.; Ezhumalai, Y.; Yang, Y.L.; Liao, C.T.; Hsu, H.F.; Wu, C. Influence of Mesogenic Properties of Cruciform-Shaped Liquid Crystals by Incorporating Side-Arms with a Laterally-Substituted-Fluorine. *Crystals* **2013**, *3*, 339–349. [CrossRef]
5. Roth, S.; Lehmann, M. Mesogenic origami–four-armed, star-shaped mesogens as precursors for functional liquid crystal materials. *Liq. Cryst.* **2017**, *44*, 1830–1851. [CrossRef]
6. Ge, L.N.; Xian, S.W.; Huang, Y.; Min, Y.; Lv, J.M.; Tian, M.; Yao, D.S. Synthesis and mesomorphism of novel multi-arm liquid crystals with cholic acid as chiral centre linking Schiff base moieties as mesogens. *Liq. Cryst.* **2018**, *45*, 1055–1067. [CrossRef]
7. Gionis, V.; Fugnitto, R.; Strzelecka, H.; Dubois, J.C. Synthesis and Properties of Mesogenic π-Donors Precursors of Mesomorphic Organic Conductors. *Mol. Cryst. Liq. Cryst.* **1983**, *96*, 215–219. [CrossRef]
8. Amilaprasadh Norbert, W.D.J.; Goodby, J.W.; Hird, M.; Toyne, K.J.; Cliff, J.J.; Patel, J.S. The Synthesis, Mesomorphic Behaviour and the Uniaxial Nature of 1,2,4,5-Tetra-(4-Alkoxybenzoyloxy) Benzenes. *Mol. Cryst. Liq. Cryst. A* **1995**, *260*, 339–350.
9. Hanna, J.-I.; Ohno, A. *Charge-Carrier Transport and Its Modeling in Liquid Crystals in Self-Organised Organic Semiconductors*; Li, Q., Ed.; Wiley: Hoboken, NJ, USA, 2011.
10. Lim, J.; Osowska, K.; Armitage, J.A.; Martin, B.R.; Miljanić, O.Š. Critical role of weak [C–H···O] hydrogen bonds in the assembly of benzo [1,2-d:4,5-d′] bisoxazole cruciforms into supramolecular sheets. *CrystEngComm* **2012**, *14*, 6152–6162.
11. Sergeyev, S.; Pisula, W.; Geerts, Y.H. Discotic liquid crystals: A new generation of organic semiconductors. *Chem. Soc. Rev.* **2007**, *36*, 1902–1929. [CrossRef]
12. Nithya, R.; Senthilkumar, K. Charge transport and optical properties of cross-conjugated organic molecules: A theoretical study. *Org. Electron.* **2014**, *15*, 1607–1623. [CrossRef]
13. Tant, J.; Geerts, Y.H.; Lehmann, M.; De Cupere, V.; Zucchi, G.; Laursen, B.W.; Bjørnholm, T.; Lemaur, V.; Marcq, V.; Burquel, A.; et al. Liquid crystalline metal-free phthalocyanines designed for charge and exciton transport. *J. Phys. Chem. B* **2005**, *109*, 20315–20323. [CrossRef]
14. Kim, B.G.; Kim, S.; Park, S.Y. Star-shaped discotic nematic liquid crystal containing 1,3,5-triethynylbenzene and oxadiazole-based rigid arms. *Tetrahedron Lett.* **2001**, *42*, 2697–2699.
15. Le Droumaguet, C.; Mongin, O.; Werts, M.V.H.; Blanchard-Desce, M. Towards "smart" multiphoton fluorophores: Strongly solvatochromic probes for two-photon sensing of micropolarity. *Chem. Commun.* **2005**, *41*, 2802–2804. [CrossRef]
16. Katan, C.; Terenziani, F.; Mongin, O.; Werts, M.H.V.; Porrès, L.; Pons, T.; Mertz, J.; Tretiak, S.; Blanchard-Desce, M. Effects of (multi) branching of dipolar chromophores on photophysical properties and two-photon absorption. *J. Phys. Chem. A* **2005**, *109*, 3024–3037. [CrossRef]
17. Holst, H.C.; Pakula, T.; Meier, H. Liquid crystals in the series of 2,4,6-tristyryl-1,3,5-triazines. *Tetrahedron* **2004**, *60*, 6765–6775.
18. Imrie, C.T.; Henderson, P.A.; Yeap, G.Y. Liquid crystal oligomers: Going beyond dimers. *Liq. Cryst.* **2009**, *36*, 755–777. [CrossRef]
19. Zhang, B.Y.; Yao, D.S.; Meng, F.B.; Li, Y.H. Structure and properties of novel three-armed star-shaped liquid crystals. *J. Mol. Struct.* **2005**, *741*, 135–140. [CrossRef]
20. Norbert, W.D.J.A.; Goodby, J.W.; Hird, M.K.; Toyne, K.J. The synthesis and mesomorphic behaviour of the 1,2,4,5-tetrasubstituted benzenes with (4-tridecyloxyphenyl)ethynyl and (4-tridecyloxyphenyl)carbonyloxy substituents. *Liq. Cryst.* **1997**, *22*, 631–642.
21. Röder, N.; Marszalek, T.; Limbach, D.; Pisula, W.; Detert, H. Tetrakis (oxadiazolylphenyl) pyrazines: New St. Andrew's Cross-Shaped Liquid Crystals. *ChemPhysChem* **2019**, *20*, 463–469. [CrossRef]
22. Hauck, M.; Schönhaber, J.; Zucchero, A.J.; Hardcastle, K.I.; Müller, T.J.J.; Bunz, U.H.F. Phenothiazine cruciforms: Synthesis and metallochromic properties. *J. Org. Chem.* **2007**, *72*, 6714–6725. [CrossRef]
23. Zucchero, A.J.; McGrier, P.L.; Bunz, U.H.F. Cross-conjugated cruciform fluorophores. *Acc. Chem. Res.* **2010**, *43*, 397–408. [CrossRef]
24. McGrier, P.L.; Solntsev, K.M.; Miao, S.; Tolbert, L.M.; Miranda, O.R.; Rotello, V.M.; Bunz, U.H.F. Hydroxycruciforms: Amine-Responsive Fluorophores. *Chem. Eur. J.* **2008**, *14*, 4503–4510. [CrossRef]
25. Xu, D.; Hao, J.; Gao, H.; Wang, Y.; Wang, Y.; Liu, X.; Han, A.; Zhang, C. Twisted donor–acceptor cruciform fluorophores exhibiting strong solid emission, efficient aggregation-induced emission and high contrast mechanofluorochromism. *Dye. Pigment.* **2018**, *150*, 293–300. [CrossRef]
26. Schmitt, V.; Moschel, S.; Detert, H. Diaryldistyrylpyrazines: Solvatochromic and acidochromic fluorophores. *Eur. J. Org. Chem.* **2013**, *2013*, 5655–5669. [CrossRef]

27. Wang, Y.; Xu, D.; Gao, H.; Wang, Y.; Liu, X.; Han, A.; Zhang, C.; Zang, L. Twisted donor–acceptor cruciform luminophores possessing substituent-dependent properties of aggregation-induced emission and mechanofluorochromism. *J. Phys. Chem. C* **2018**, *122*, 2297–2306. [CrossRef]
28. Meti, P.; Yang, J.W.; Gong, Y.D. Aggregation induced emission properties of cruciform-type conjugated pyrazine molecules with four pendent donor groups. *Dye. Pigment.* **2021**, *192*, 109419. [CrossRef]
29. Wöhrle, T.; Wurzbach, I.; Kirres, J.; Kostidou, A.; Kapernaum, N.; Litterscheidt, J.; Haenle, J.C.; Staffeld, P.; Baro, A.; Giesselmann, F.; et al. Discotic liquid crystals. *Chem. Rev.* **2016**, *116*, 1139–1241. [CrossRef]
30. Kumar, S. *Chemistry of Discotic Liquid Crystals*; CRC Press: Boca Raton, FL, USA, 2016. [CrossRef]
31. Ito, S.; Inabe, H.; Morita, N.; Ohta, K.; Kitamura, T.; Imafuku, K. Synthesis of poly(6-azulenylethynyl)benzene derivatives as a multielectron redox system with liquid crystalline behavior. *J. Am. Chem. Soc.* **2003**, *125*, 1669–1680. [CrossRef]
32. Hayer, A.; De Halleux, V.; Köhler, A.; El-Garoughy, A.; Meijer, E.W.; Barberá, J.; Tant, J.; Levi, J.; Lehmann, M.; Gierschner, J.; et al. Highly fluorescent crystalline and liquid crystalline columnar phases of pyrene-based structures. *J. Phys. Chem. B* **2006**, *110*, 7653–7659. [CrossRef]
33. Hsu, H.F.; Chen, H.C.; Kuo, C.H.; Wang, B.C.; Chiu, H.T. Design and investigation of calamitic liquid crystals with low aspect-ratios: Rigid y-shaped 1,2,4-tris(4-alkoxyphenylethynyl)benzenes. *J. Mater. Chem.* **2005**, *15*, 4854–4861.
34. Schultz, A.; Laschat, S.; Diele, S.; Nimtz, M. Tetraphenylethene-Derived Columnar Liquid Crystals and Their Oxidative Photocyclization. *Eur. J. Org. Chem.* **2003**, *2003*, 2829–2839. [CrossRef]
35. Chaudhuri, R.; Su, M.Y.; Li, C.W.; Wang, C.I.; Chen, C.J.; Lai, C.K.; Chen, L.Y.; Liu, S.H.; Wu, C.C.; Liu, R.S. Functionalized dibenzo[g,p] chrysenes: Variable photophysical and electronic properties and liquid–crystal chemistry. *Org. Lett.* **2008**, *10*, 3053–3056. [CrossRef]
36. Li, H.; Valiyaveettil, S. Synthesis and characterization of cross-conjugated cruciforms with varied functional groups. *Tetrahedron Lett.* **2009**, *50*, 5311–5314. [CrossRef]
37. Alibert-Fouet, S.; Seguy, I.; Bobo, J.-F.; Destruel, P.; Bock, H. Liquid-Crystalline and Electron-Deficient Coronene Oligocarboxylic Esters and Imides By Twofold Benzogenic Diels–Alder Reactions on Perylenes. *Chem.-Eur. J.* **2007**, *13*, 1746–1753. [CrossRef]
38. Thiebaut, O.; Bock, H.; Grelet, E. Face-on Oriented Bilayer of Two Discotic Columnar Liquid Crystals for Organic Donor–Acceptor Heterojunction. *J. Am. Chem. Soc.* **2010**, *132*, 6886–6887. [CrossRef]
39. Detert, H.; Sugiono, E.; Kruse, G. Solvent-dependent fluorescence of donor-substituted (E)-1,2-bis(stilbenyl-1,3,4-oxadiazolyl) ethenes. *J. Phys. Org. Chem.* **2002**, *15*, 638–641.
40. Girotto, E.; Eccher, J.; Vieira, A.A.; Bechtold, I.H.; Gallardo, H. Luminescent columnar liquid crystals based on 1,3,4-oxadiazole. *Tetrahedron* **2014**, *70*, 3355–3360.
41. Huisgen, R.; Sauer, J.; Sturm, H.J.; Markgraf, J.H. Ringöffnungen der Azole, II. Die Bildung von 1.3.4-Oxdiazolen bei der Acylierung 5-substituierter Tetrazole. *Chem. Ber.* **1960**, *93*, 2106–2124. [CrossRef]
42. Pradhan, B.; Pathak, S.K.; Gupta, R.K.; Gupta, M.; Pal, S.K.; Achalkumar, A.S. Star-shaped fluorescent liquid crystals derived from s-triazine and 1,3,4-oxadiazole moieties. *J. Mater. Chem. C* **2016**, *4*, 6117–6130.
43. Curtius, T.; Dellschaft, F.H. Hydrazide und Azide organischer Säuren. *J. Prakt. Chem.* **1901**, *64*, 419–438. [CrossRef]
44. Tober, N.; Rieth, T.; Lehmann, M.; Detert, H. Synthesis, Thermal, and Optical Properties of Tris (5-aryl-1,3,4-oxadiazol-2-yl)-1,3,5-triazines, New Star-Shaped Fluorescent Discotic Liquid Crystals. *Chem. Eur. J.* **2019**, *25*, 15295–15304.
45. Cantillo, D.; Gutmann, B.; Kappe, C.O. An experimental and computational assessment of acid-catalyzed azide-nitrile cycloadditions. *J. Org. Chem.* **2012**, *77*, 10882–10890. [CrossRef]
46. Dürr, M.; Klein, J.; Kahnt, A.; Becker, S.; Puchta, R.; Sarkar, B.; Ivanović-Burmazović, I. Redox behavior of a dinuclear ruthenium (II) complex bearing an uncommon bridging ligand: Insights from high-pressure electrochemistry. *Inorg. Chem.* **2017**, *56*, 14912–14925. [CrossRef]
47. Schollmeier, D.; Detert, H. (E)-1,2-Bis (5-aryl-1,3,4-oxadiazol-2-yl) ethenes. *Synthesis* **1999**, *1999*, 999–1004.
48. Kumar, S. Self-organization of disc-like molecules: Chemical aspects. *Chem. Soc. Rev.* **2006**, *35*, 83–109. [CrossRef]
49. Hestand, N.J.; Spano, F.C. Expanded theory of H-and J-molecular aggregates: The effects of vibronic coupling and intermolecular charge transfer. *Chem. Rev.* **2018**, *118*, 7069–7163. [CrossRef]
50. Graschtat, V.; Proz, I.; Lehmann, M.; Detert, H. 1,2,4-Tris (5-aryl-1,3,4-oxadiazolyl)-benzenes: Novel λ-shaped fluorescent liquid crystals. *J. Mater. Chem. C* **2025**, *13*, 15941–15947.
51. Rieth, T.; Tober, N.; Limbach, D.; Haspel, T.; Sperner, M.; Schupp, N.; Wicker, P.; Glang, S.; Lehmann, M.; Detert, H. Impact of substitution pattern and chain length on the thermotropic properties of alkoxy-substituted triphenyl-tristriazolotriazines. *Molecules* **2020**, *25*, 5761. [CrossRef]